Inorg. Chem. **2009**, *48*, 446−454

Conjugated Organometallic Polymer Containing a Redox-Active Center

Daniel Fortin,*,† Sébastien Clément,† Karl Gagnon,† Jean-François Bérubé,† Michael P. Stewart,‡ William E. Geiger,‡ and Pierre D. Harvey*,†

Département de Chimie, Université de Sherbrooke, 2550 Boul. Université, Sherbrooke, PQ, Canada J1K 2R1, and Department of Chemistry, University of Vermont, Burlington, Vermont 05405

Received May 12, 2008

The new conjugated organometallic polymer (−spacer−C≡C−Pt(PBu_3)$_2$−C≡C−)$_n$ (**3**; spacer = *para*-bis(diphenyl-(tetramethyl)quinone diimine) and the cyclic mononuclear model complex, spacer′−C≡C−Pt(PEt_3)$_2$−C≡C · CuCl (**4**; spacer′ = *ortho*-diphenyl-2,3,5,6-tetramethyl-1,4-benzoquinone diimine) were synthesized from the 1:1 condensation of the corresponding diethynyl ligands (**2-para** and **2-ortho** (*para*- and *ortho*-diethynyl-diphenyl-2,3,5,6-tetramethylquinone diimine), respectively), with the *trans*-Pt(PBu_3)$_2$$Cl_2$ for polymer **3** and *cis*-Pt(PEt_3)$_2$$Cl_2$ for **4**. The materials were characterized by GPC, DSC, ATG, and electrochemistry for polymer **3**, and by X-ray diffraction for **4**. Polymer **3** exhibits a M_n of 18500, M_w of 25000 with a PD of 1.37. The *trans*-geometry about Pt in polymer **3** was confirmed by ^{31}P NMR and IR/Raman spectroscopy. The cyclic voltammogram study on the model complex *trans*-Pt(PBu_3)$_2$(C≡CPh)$_2$, spacer **1-para** (Me_3Si−C≡C−R−C≡C−$SiMe_3$; R = *para*-diphenyl-2,3,5,6-tetramethyl-1,4-benzoquinone diimine) and polymer **3** demonstrated that polymer **3** in the presence of trifluoroacetic acid (TFA) exhibits a quasi reversible 2-electron reduction process centered at 0.48 V versus SCE corresponding to the reduction of the protonated quinone diimine unit into the corresponding diamine. The UV−vis spectra of the spacer **2-para** (440 nm) and polymer **3** (502 nm) are characterized by red-shifted charge transfer (CT) absorptions (C_6H_4C≡C → quinone diimine for **2-para**; and (C_6H_4C≡C)$_2$Pt → quinone diimine for polymer **3**). These assignments are corroborated by density-functional theory (DFT) and time-dependent density-functional theory (TDDFT) computations. Polymer **3** is not luminescent in the solid state or in solution at 77 K and 298 K.

Introduction

During past several years, we witnessed tremendous progress in the design of semi- and photoconducting and optical materials (including photovoltaic cells).[1] Among the building blocks for the preparation of these materials, metal-containing molecules were the subject of intense research.[2] The insertion of a metal center into the polymeric chain contributes to the delocalized π-electron system and often gives electronic interaction between the transition metal and the organic molecular framework leading to the possibility of optical transitions that do not occur in organic compounds such as d-d electronic transitions, metal-to-ligand-charge-transfer, and ligand-to-metal-charge-transfer, as well as promoting intersystem crossing to generate triplet states.[3] An interesting class of such organometallic conjugated polymers includes the platinum(II) σ-alkynyl complexes.[2] These materials often exists as polymetallaynes of the type *trans*-[−PtL_2−C≡C−Ar−C≡C−]$_n$ with a wide variety of aromatic ring (Ar) systems. Their electronic and optical properties can be fine-tuned by variation of the aromatic spacers of the organic ligands and the auxiliary ligands on the metal. For example, introduction of a redox active spacer brings the possibility of introducing charges or electron vacancies along the conjugated chain (mixed-valence), hence promoting electron delocalization along the polyalkyne

* To whom correspondence should be addressed. E-mail: pierre.harvey@usherbrooke.ca. Phone: (819) 821-7092. Fax: (819) 821-8017.
† Université de Sherbrooke.
‡ University of Vermont.

(1) (a) Leroux, Y. R.; Lacroix, J. C.; Chane-Ching, K. I.; Fave, C.; Felidj, N.; Levi, G.; Aubard, J.; Krenn, J. R.; Hohenau, A. *J. Am. Chem. Soc.* **2005**, *127*, 16022–16023. (b) Seminario, J. M.; De La Cruz, C.; Derosa, P. A.; Yan, L. *J. Phys. Chem. B.* **2004**, *108*, 17879–17885. (c) Kwong, R. C.; Sibley, S.; Dubovoy, T.; Baldo, M.; Forrest, S. R.; Thompson, M. E. *Chem. Mater.* **1999**, *11*, 3709–3713. (d) Hissler, M.; McGarrah, J. E.; Connick, W. B.; Geiger, D. K.; Cummings, S. D.; Eisenberg, R. *Coord. Chem. Rev.* **2000**, *208*, 115–137. (e) Zhou, G.-J.; Wang, X.-Z.; Wong, W.-Y.; Yu, X.-M.; Kwok, H.-S.; Lin, Z. *J. Organomet. Chem.* **2007**, *692*, 3461–3473.

10.1021/ic800857v CCC: $40.75
Published on Web 11/25/2008

Scheme 1

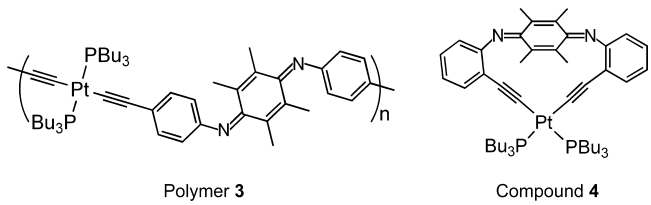

chains. In a previous work,[4] we reported a series of polymers of the type (-(quinone diimine)-[metal]-)$_n$ where [metal] is either the *cis*- or *trans*-Pt$(PEt_3)_2(C{\equiv}CC_6H_4)_2$ and the quinone diimine moiety is the *ortho*- or *para*-substituted *N*,*N*′-tetramethoxyquinone diimine. The quinone diimine skeleton is especially interesting since it exhibits electro-responsive properties in acidic solution[5] and can be related to the well-known, conductive polymer polyaniline (PANI),[6] in its protonated emeraldine form. Unfortunately, the presence of acid did not generate the protonated form because the methoxy groups acted as proton receptors competing with the imine centers, and at larger concentrations, decomposition occurred.

We now wish to report the synthesis of the platinum-containing **polymer 3** of the type (-(ethynylbenzene)-(quinone diimine)-(ethynylbenzene)-[metal]-)$_n$ where [metal] is *trans*-Pt$(PBu_3)_2$ and (quinone diimine) is *para*-substituted bis(ethynylbenzene)-*N*,*N*′−2,3,5,6-tetramethyl-1,4-benzoquinone diimine (Scheme 1). During the course of this study, the cyclic model compound **4** (i.e., 1 unit) was also prepared and characterized. Indeed, polymer **3** exhibits a chemically reversible electrochemical redox system.

Experimental Section

Materials. Compound *trans*-Pt$(PBu_3)_2Cl_2$,[7] *trans*-Pt$(PEt_3)_2Cl_2$,[8] *trans*-Pt$(PBu_3)_2(C{\equiv}CPh)_2$ (**5**),[9] and 4-[(trimethylsilyl)ethynylaniline][10] were prepared according to literature procedures. $TiCl_4$ (Aldrich), CuI (Aldrich), trimethylsilylacetylene (Fluka), duroquinone (Aldrich), 4-bromoaniline (Aldrich) 2-[(trimethylsilyl)-ethynylaniline] (Aldrich), tetrabutylammonium hexafluorophosphate (Aldrich) were commercially available and were used as received. All reactions were performed in Schlenk-tube flasks under purified nitrogen. All flasks were dried under a flame to eliminate moisture. All solvents were distilled from appropriate drying agents.

2,3,5,6-Tetramethyl-*N*,*N*′-bis(*para*-trimethylsilylethynylphenyl)-1,4-benzoquinone Diimine (1-para). Thirty milliliters of chlorobenzene was placed in a three-necked round bottomed flask. A 0.76 g quantity (4.0 mmol) of 4-[(trimethylsilyl)ethynyl]aniline, 1.13 mL (8.0 mmol) of triethylamine, and 0.57 g (3.0 mmol) of $TiCl_4$ were added to the flask using a syringe. A 0.33 g quantity (2.0 mmol) of duroquinone was dissolved in a minimum amount of chlorobenzene and added dropwise to the solution. The solution was stirred at 60 °C for 4 h. The mixture was left to cool to room temperature, filtered, and washed with chlorobenzene. The solution was evaporated. The solid was dissolved in CH_2Cl_2, washed three times with water, dried with $MgSO_4$, and filtered. The CH_2Cl_2 was completely evaporated leaving only the product. The product was purified on a silica column with CH_2Cl_2/hexane (30:70) as the solvent to give disilylated compound **1-para**. (0.69 g, 68%). IR (KBr): 2156 ($\nu_{C\equiv C}$) cm^{-1}. ^{1}H NMR ($CDCl_3$): δ 0.24 (18 H, s, $Si(CH_3)_3$), 1.42 (6 H, br. s, CH_3); 2.17 (6 H, br. s, CH_3,); 6.75 (4 H, d, CH aro., $^3J_{H-H}$ = 8.0); 7.40 (4 H, d, CHaro., $^3J_{H-H}$ = 8.0). UV−vis(2-MeTHF) (λ_{max} nm (ε)): 277 (23100), 306 (23500); 446 (5690 M^{-1}.cm^{-1}). ESI MS: m/z = 508 [M$^+$ + 2H]. Red prism crystals suitable for X-ray diffraction were grown by slow evaporation of a DMF solution at room temperature. The monosubstituted derivative 2,3,5,6-tetramethyl-(*ortho*-trimethylsilylethynylphenyl)-iminequinone (**1′-para**) was also isolated during the synthesis of **1-para**. IR (KBr): 2156 ($\nu_{C\equiv C}$) 1588 ($\nu_{C=N}$) cm^{-1}.^{1}H NMR (CD_2Cl_2): δ 7.25 (2 H, d, Ph, $^3J_{H-H}$ = 7.6); 6.48 (2 H, d, Ph, $^3J_{H-H}$ = 7.6); 2.12 (6 H, s, CH_3), 1.98 (6 H, s, CH_3); 0.21 (9 H, s, $Si(CH_3)_3$). ESI MS: m/z = 335 [M$^+$]. Anal. Calcd for $C_{21}H_{25}NOSi$ C, 75.18; H, 7.51; N, 4.17; Found: C, 75.30; H, 7.65; N, 4.35. Pink prism crystals suitable for X-ray diffraction were grown by slow evaporation of a CH_2Cl_2/MeOH (75:25) solution at room temperature.

2,3,5,6-Tetramethyl-*N*,*N*′-bis(*ortho*-trimethylsilylethynylphenyl)-1,4-benzoquinone Diimine (1-ortho). 1-ortho is synthesized in a similar manner as **1-para**. Purification of the residue by column chromatography on silica gel with hexane/toluene (20:80) gave **1-ortho** as a red powder (0.94 g, 75%). IR (KBr): 2151 ($\nu_{C\equiv C}$), 1586 ($\nu_{C=N}$) cm^{-1}. ^{1}H NMR (CD_2Cl_2): δ 7.43 (4 H, d, Ph, $^3J_{H-H}$ = 7.65); 7.24 (4 H, d, Ph, $^3J_{H-H}$ = 7.65); 6.99 (4 H, t, Ph, $^3J_{H-H}$= 7.53); 6.51 (4 H, br. s, Ph); 1.92 (12 H, br. m, CH_3); 0.19 (18 H, s, $Si(CH_3)_3$). ^{13}C{^{1}H} NMR (CD_2Cl_2): δ 146.0 (*C*=N), 134,1, 131.6, 122.0, 114.6, 112.0, 103.9, 102.3 (Ph), 31.6 (CH_3), 1.5 ($Si(CH_3)_3$). ESI MS: m/z = 506 [M+]. Red prism crystals suitable for X-ray diffraction were grown by slow evaporation of a DMF solution at room temperature. The monosubstituted derivative 2,3,5,6-tetramethyl-(*ortho*-trimethylsilyl-ethynylphenyl)iminequinone (**1′-ortho**) was also isolated during the synthesis of **1-ortho**. IR (KBr): 2156 ($\nu_{C\equiv C}$), 1590 ($\nu_{C=N}$) cm^{-1}. ^{1}H NMR (CD_2Cl_2): δ 7.40 (2 H, d, Ph, $^3J_{H-H}$ = 7.7); 7.28 (2 H, t, Ph, $^3J_{H-H}$ = 7.7); 6.99 (2 H, t, Ph,

(2) (a) Wong, W.-Y. *J. Inorg. Organomet. Polym. Mater.* **2005**, *15*, 197–217. (b) Singh, C. P.; Kulshresta, K.; Roy, S. *Optik* **2006**, *117*, 499–504. (c) Glimsdal, E.; Carisson, M.; Eliasson, B.; Minaev, B.; Lindgren, M. *J. Phys. Chem. A* **2007**, *111*, 244–250. (d) Wong, W.-Y. *Coord. Chem. Rev.* **2007**, *251*, 2400–2427. (e) Herbert, D. E.; Mayer, U. F. J. *Angew. Chem., Int. Ed.* **2007**, *46*, 5060–5081. (f) Williams, K. A.; Boydston, A. J.; Bielawski, C. W. *Chem. Soc. Rev.* **2007**, *36*, 729–744. (g) Wong, W.-Y.; Wang, X.-Z.; He, Z.; Djurìsic, A. B.; Yip, C.-T.; Cheung, K.-Y.; Wang, H.; Mak, C. S.; Chan, K. W.-K. *Nat. Mater.* **2007**, *6*, 521–527.

(3) (a) Lindgren, M.; Minaev, B.; Glimsdal, E.; Vestberg, R.; Westlund, R.; Malmstrom, E. *J. Lumin.* **2007**, *124*, 302–310. (b) Wong, W.-Y.; Liu, L.; Poon, S.-Y.; Choi, K.-H.; Cheah, K.-W.; Shi, J.-X. *Macromolecules* **2004**, *37*, 4496–4504. (c) Fyfe, H. B.; Mlekuz, M.; Stringer, G.; Taylor, N. J.; Marder, T. B. *Inorganic and organometallic polymers with special properties*; Laine, R. M., Ed.; Kluwer Academic Publishers: Dordrecht, The Netherlands, 1992; pp 331. (d) Long, N. J.; Williams, C. K. *Angew. Chem., Int. Ed.* **2003**, *42*, 2586–2617.

(4) Gagnon, K.; Aly, S. M.; Brisach-Wittmeyer, A.; Bellows, D.; Berube, J.-F.; Caron, L.; Abd-El-Aziz, A. S.; Fortin, D.; Harvey, P. D. *Organometallics* **2008**, *27*, 2201–2214.

(5) (a) Nishiumi, T.; Chimoto, Y.; Hagiwara, Y.; Higuchi, M.; Yamamoto, K. *Macromolecules* **2004**, *37*, 2661–2664. (b) Nishiumi, T.; Nomura, Y.; Chimuto, Y.; Higuchi, M.; Yamamoto, K. *J. Phys. Chem. B* **2004**, *108*, 7992–8000. (c) Han, C.-C.; Balakumar, R.; Thirumalai, D.; Chung, M.-T. *Org. Biomol. Chem.* **2006**, *4*, 3511–3516.

(6) (a) Wolf, J. F.; Forbes, C. E.; Gould, S.; Shacklette, L. W. *J. Electrochem. Soc.* **1989**, *136*, 2887–2891. (b) Lux, F. *Polymer* **1994**, *35*, 2915–36. (c) Davies, S. J.; Ryan, T. G.; Wilde, C. J.; Beyer, G. *Synth. Met.* **1995**, *69*, 209–10. (d) Pelster, R.; Nimtz, G.; Wessling, B. *Phys. Rev. B: Condens. Matter* **1994**, *49*, 12718–23. (e) Hagiwara, T.; Demura, T.; Iwata, K. *Mater. Sci.* **1987**, *13*, 87–90.

(7) Kauffmann, G. B.; Teterm, L. A. *Inorg. Synth.* **1963**, *7*, 245–249.

(8) Parshall, G. W. *Inorg. Synth.* **1970**, *12*, 26–33.

(9) Liu, Y.; Jiang, S.; Glusac, K.; Powell, D. H.; Anderson, D. F.; Schanze, K. S. *J. Am. Chem. Soc.* **2002**, *124*, 12412–12413.

(10) Hundertmark, T.; Litke, A. F.; Buchwald, S. L.; Fu, G. C. *Org. Lett.* **2000**, *2*, 1729–1731.

$^3J_{H-H}$ = 7.6); 6.72 (2 H, d, Ph, $^3J_{H-H}$ = 8.0); 1.97 (12 H, m, CH_3); 0.08 (9 H, s, $Si(CH_3)_3$). $^{13}C\{^1H\}$ NMR (CD_2Cl_2): δ 188.1 (*C*=O), 161.0 (*C*=N), 155.8, 138.8, 134.2, 124.9, 119.4, 112.8, 103.8, 100.2 (Ph), 18.0, 13.9 (*C*H_3), 1.3 ($Si(CH_3)_3$). ESI MS: *m*/*z* = 335 [M+]. Anal. Calcd for $C_{21}H_{25}NOSi$ C, 75.18; H, 7.51; N, 4.17; Found: C, 75.32; H, 7.68; N, 4.30. Red prism crystals suitable for X-ray diffraction were grown by slow evaporation of a CH_2Cl_2/MeOH (75:25) solution at −10 °C.

2,3,5,6-Tetramethyl-*N*,*N*′-bis(*para*-ethynylbenzene)-1,4-benzoquinone Diimine (2-para). A 0.51 g quantity (1.0 mmol) of **1-para** was placed in a 250 mL round-bottomed flask, and 7 g of K_2CO_3 was added to the flask, as well as 200 mL of CH_3OH. The reaction was stirred under Ar overnight until the solution had become orange. The excess K_2CO_3 was filtered, and the remaining solvent was evaporated. The residue was dissolved in CH_2Cl_2 and washed three times with water. The CH_2Cl_2 solution was dried with K_2CO_3 and filtered. The product was purified on a silica column with ethyl acetate/hexanes (20:80) as eluant to give **2-para** as a red powder (0.28 g, 78%). IR (KBr): 3292 ($\nu_{\equiv CH}$), 2103 ($\nu_{C\equiv C}$), 1582 ($\nu_{C=N}$) cm^{-1}. ^{1}H NMR ($CDCl_3$): δ 7.45 (4H, d, CH aro., $^3J_{H-H}$= 8.8); 6.76 (4 H, d, CH aro., $^3J_{H-H}$ = 8.8); 3.07 (2H, s, ≡CH); 2.17 (6 H, br s, CH_3); 1.44 (6 H, br s, CH_3). $^{13}C\{^1H\}$ NMR ($CDCl_3$): δ 151.9 (*C*=N), 132.9−119.7, 117.0 (Ph), 83.8, 76.7 (C≡C); 14.8, 14.2 (*C*H_3). UV−vis(2-MeTHF) (λ_{max} nm (ε)): 268 (27700), 306 (35300), and 440 (7100 M^{-1}.cm^{-1}). Anal. Calcd for $C_{26}H_{22}N_2$ C, 86.15; H, 6.12; N, 7.73; Found: C, 86.34; H, 6.29; N, 7.75.

2,3,5,6-Tetramethyl-*N*,*N*′-bis(*ortho*-ethynylbenzene)-1,4-benzoquinone Diimine (2-ortho). 2-ortho was synthesized in a similar manner as **2-para** and was isolated as an orange powder (0.182 g, 76%). IR (KBr): 3294 ($\nu_{\equiv CH}$), 2100 ($\nu_{C\equiv C}$), 1588 ($\nu_{C=N}$) cm^{-1}. ^{1}H NMR (CD_2Cl_2): δ 7.47 (4 H, d, Ph, $^3J_{H-H}$ = 7.7); 7.28 (4 H, t, Ph, $^3J_{H-H}$ = 7.7); 7.02 (4 H, t, Ph, $^3J_{H-H}$ = 7.5); 6.66 (4 H, m, Ph); 1.97 (14 H, m, CH_3 and C≡C*H*). $^{13}C\{^1H\}$ NMR ($CDCl_3$): δ 156.0 (*C*=N), 134.9, 134.5, 132.1, 131.4, 120.4, 118.7, 112.6 (Ph), 85.1, 83.2 (C≡C), 16.9 (CH_3). ESI MS: *m*/*z* = 362 [M+]. Anal. Calcd for $C_{26}H_{22}N_2$ C, 86.15; H, 6.12; N, 7.73; Found: C, 85.95; H, 6.01; N, 7.64.

Poly(2,3,5,6-tetramethyl-*N*,*N*′-bis(*para*-ethynylbenzene)-1,4-benzoquinone Diimine)-*trans*-bis(tributylphosphine)platinum(II) (polymer 3). A 0.09 g quantity (0.25 mmol) of **2-para**, 0.17 g (0.25 mmol) of *trans*-$Pt(PBu_3)_2Cl_2$, and 0.01 g of CuI were dissolved in 10 mL of CH_2Cl_2. Ten millilters of $^iPr_2NH$ were added, and the reaction was stirred under Ar overnight. The solvent was evaporated. The residue was dissolved in CH_2Cl_2 and washed three times with water. The solution of CH_2Cl_2 was dried with K_2CO_3 and filtered. The solvent was then evaporated, and polymer **3** was obtained as a red powder. The polymer was reprecipitated in dichloromethane by adding hexane (0.20 g, 83%). IR (KBr): 2097 ($\nu_{C\equiv C}$), 1573 ($\nu_{C=N}$) cm^{-1}. $^{31}P\{^1H\}$ NMR ($CDCl_3$): δ 6.91 (2P, s, $^1J_{Pt-P}$ = 2360). ^{1}H NMR ($CDCl_3$): δ 7.22 (4H, d, CH aro., $^3J_{H-H}$ = 7.4); 6.69 (4H, d, CH aro., $^3J_{H-H}$ = 7.4); 2.15 (18H, br m, CH_2 + =C−CH_3); 1.62 (12H, br m, CH_2), 1.42 (18H, br m, CH_2 + =C−CH_3), 0.92 (18H, t, CH_3, $^3J_{H-H}$ = 7.1). $^{13}C\{^1H\}$ NMR ($CDCl_3$): δ 131.4−120.1 (Ph), 108.2 (C≡C), 26.2, 24.5, 23.9 (CH_2); 14.5, 13.8 (CH_3). UV−vis(2-MeTHF) (λ_{max} nm (ε)): 298 (42300), 336 (58800), 502 (23400 M^{-1} cm^{-1}). Anal. Calcd for $C_{50}H_{74}N_2P_2Pt$ C, 62.55; H, 7.77; N, 2.92; Found: C, 62.32; H, 7.98; N, 3.14.

Chlorocopper(I)-cyclo(2,3,5,6-tetramethyl-*N*,*N*′-bis(*ortho*-ethynylbenzene)-1,4-benzoquinone Diimine)bis(triethylphosphine)-platinum(II) (4). 2-ortho (0.18 g, 0.50 mmol) was placed in a 100 mL round-bottom flask with *cis*-$Pt(PEt_3)_2Cl_2$ (0.25 g, 0.50 mmol) and CuI (30 mg). CH_2Cl_2 (30 mL) and diisopropylamine (30 mL) were added. The mixture was stirred and kept away from the light during 1 day and then filtered. The solvent was reduced under reduced pressure. Purification of the residue was performed by recrystallization in DMF to afford **4** as dark red crystals (0.29 g, 65%). IR (KBr): 2103 ($\nu_{C\equiv C}$) cm^{-1}. $^{31}P\{^1H\}$ NMR (CD_2Cl_2): δ 8.14 (2 P, s, $^1J_{Pt-P}$ = 1120). ^{1}H NMR (CD_2Cl_2): 6.90 (m, 8 H, Ph); 2.01 (m, 12 H, CH_2); 1.20 (m, 18 H, CH_3). $^{13}C\{^1H\}$ NMR ($CDCl_3$): δ 123.8, 121.0, 111.6 (Ph), 49.2 (CH_2), 21.0, 10.0 (CH_3); Anal. Calcd for $C_{38}H_{50}N_2PtP_2CuCl\cdot$DMF C, 51.09; H, 5.96; N, 4.36; Found: C, 50.95; H, 5.80; N, 4.20. The presence of DMF was also found in the X-ray structure. Red plate crystals suitable for X-ray diffraction were grown by slow evaporation of a DMF solution at room temperature.

Instruments. All NMR spectra were acquired on a Bruker AC-300 spectrometer (^{1}H 300.15 MHz, ^{13}C 75.48 MHz, ^{31}P 121.50 MHz) using the solvent as chemical shift standard, except in ^{31}P NMR, where the chemical shifts are relative to D_3PO_4 85% in D_2O. All chemical shifts (δ) and coupling constants (*J*) are given in ppm and Hertz, respectively. The spectra were measured from freshly prepared samples. The IR spectra were acquired on a Bomem FT-IR MB series spectrometer equipped with a baseline-diffused reflectance. Raman spectra were recorded on a Bruker RFS 100/S spectrometer with the 1064 nm excitation and a light power equal to 0.50 W. UV−visible spectra were recorded on a Hewlett-Packard diode array model 8452A. Emission and excitation spectra were obtained using a double monochromator Fluorolog 2 instrument from Spex. Fluorescence lifetimes were measured on a Timemaster Model TM-3/2003 apparatus from PTI. Some phosphorescence lifetime measurements and time-resolved spectra were also performed on a PTI LS-100 using a 1 μs tungsten-flash lamp. The source was nitrogen laser with high-resolution dye laser (fwhm ∼ 1.5 ns) and the fluorescence lifetimes were obtained from high quality decays and deconvolution or distribution lifetimes analysis. The uncertainties were about ±10−40 ps based on multiple measurements. Quantum yield of 2-para was calculated by using 9,10-diphenylanthracene (Φ = 1.0) as comparative standard.[11]

Gel Permeation Chromatography. Molecular weight and molecular weight distributions of polymer **3** were determined by using gel permeation chromatography (GPC). The GPC setup consisted of a Waters 515 HPLC pump, a Waters 996 Photodiode Array Detector, and a Waters 410 Differential Refractometer, with a Styragel HR4E column (7.8 × 300 mm). The GPC eluent was HPLC grade THF, at a flow rate of 0.5 mL min^{-1}. The calibration curve was obtained using seven PS standards (Aldrich), with Mn ranging from 3400 to 382 000 g mol^{-1}.

Electrochemistry. Electrochemical measurements were carried out at room temperature under a flow of nitrogen gas. DMF (EMD) was stored over type 4A molecular sieves for several days but otherwise used as received. Trifluoroacetic acid (EMD, 99.5%), TFA, was used as received. Solutions were made 0.1 M in $[NBu_4][PF_6]$, which had been purchased from TCI, recrystallized from ethanol, and vaccuum-dried. Electrochemical experiments were carried out using a standard three-electrode configuration and a PARC 273A potentiostat interfaced to a personal computer. The compounds in this paper exhibited more consistent voltammetric behavior at Pt working electrodes, compared to their behavior at glassy carbon or gold, so that cyclic voltammetry (CV) and differential pulse voltammetry (DPV) scans were carried out at Pt disks of 1 or 2 mm diameter (Bioanalytical Systems) which had been polished with Buehler diamond paste. The potentials are reported versus the saturated calomel electrode (sce) to be consistent

(11) Morris, J. V.; Mahaney, M. A.; Huber, J. R. *J. Phys. Chem.* **1976**, *80*, 969–974.

Table 1. X-ray Crystallographic and Refinement Data for **1-para**, **1-ortho**, and **4**

	1-para	**1-ortho**	**4**
formula	$C_{32}H_{38}N_2Si_2$	$C_{32}H_{38}N_2Si_2$	$C_{41}H_{57}ClCuN_3OP_2Pt$
FW ($g.mol^{-1}$)	506.82	506.82	963.92
T (K)	198(2) K	293(2) K	198(2) K
crystal system	monoclinic	monoclinic	monoclinic
space group	*C2/c*	*P21*	*P2(1)/c*
a (Å)	37.042(17)	9.704(4) Å	10.169(2)
b (Å)	10.002(3)	10.838(11) Å	25.404(5)
c (Å)	10.002(3)	14.659(11) Å	11.609(2)
α (deg)	90	90	90
β (deg)	101.90(5)	91.28(5)	112.30(4)
γ (deg°)	90	90	90
V (Å^3)	6339(6)	1541(2)	4072(5)
Z	8	2	4
ρ_{calc} ($mg.m^{-3}$)	1.062	1.092	1.572
μ (mm^{-1})	1.159	1.192	1.107
F(000)	2176	544	720
Θ range (deg)	2.44−69.93	3.02−69.88	2.34 to 70.54
index ranges	$0 \le h \le 44$	$-11 \le h \le 11$	$-24 \le h \le 22$
	$-12 \le k \le 0$	$0 \le k \le 13$	$0 \le k \le 12$
	$-21 \le l \le 20$	$0 \le l \le 17$	$0 \le l \le 26$
collected reflections	5894	2797	6572
independent reflections	5894 [R(int) = 0.0000]	2797 [R(int) = 0.0000]	6572 [R(int) =0.000]
data/restraints/parameters	5894/0/336	2797/1/331	6572/0/398
largest differences in peak and hole ($e.Å^{-3}$)	0.215 and−0.331	0.448 and −0.229	0.231 and −0.347
final R indices [$I > 2\sigma(I)$]	R1 = 0.0730; wR2 = 0.1785	R1 = 0.0913; wR2 = 0.2343	R1 = 0.1033; wR2 = 0.2596
R indices (all data)	R1 = 0.1514; wR2 = 0.2134	R1 = 0.1328; wR2 = 0.2675	R1 = 0.2018; wR2 = 0.3270
GOF on F^2	0.947	1.004	1.182

Scheme 2. Synthesis of the Diethynyl Ligands **2**

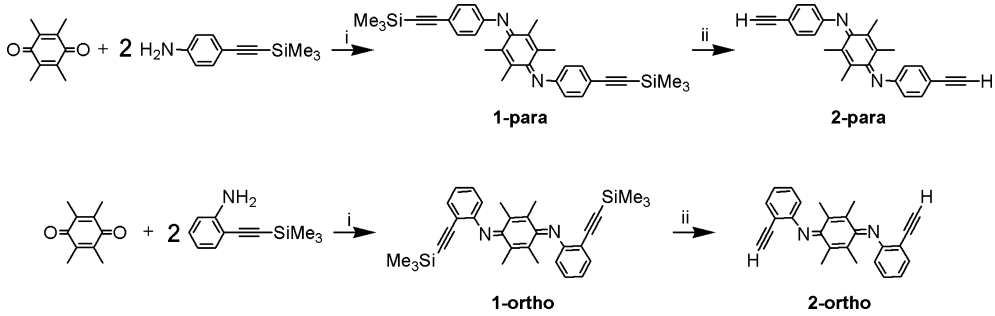

with an earlier paper,[4] but the *in situ* approach using a ferrocene internal reference was used to obtain the values, which were then converted to sce by addition of 0.45 V.[12]

Crystallography. Data were collected on an Enraf-Nonius CAD-4 automatic diffractometer at 198(2) K (**1-para**, **1-ortho**, **1′-para**, **1′-ortho**) and 293(2) K (**4**) using ω scans. The DIFRAC[13] program was used for centering, indexing, and data collection. One standard reflection was measured every 100 reflections, and no intensity decay was observed during data collection. The data were corrected for absorption by empirical methods based on psi scans and reduced with the NRCVAX[13] programs. They were solved using SHELXS-97[14] and refined by full-matrix least-squares on F^2 with SHELX-97.[15] The non-hydrogen atoms were refined anisotropically. The hydrogens atoms were placed at idealized calculated geometric position and refined isotropically using a riding model. The absolute structure of **1-ortho** was determined by anomalous dispersion effects.[16] For cyclic compound **4**, the crystal was twinned so the bad reflections were taken out the final refinement, and this is why the observed/unique ratio is low. The theta completeness ratio for **1′-ortho** is low because some bad reflections had to be omitted because of the poor quality of the crystal. The crystal data of **1-para, 1-ortho** and **4** are placed in Table 1.

Computations. All calculations were performed on an Intel Xeon 3.40 GHz PC with the Gaussian 03, revision C.02, and Gausview 3.0 software packages.[17] The hybrid B3LYP exchange-correlation function has been considered because of the high accuracy of the ensued results.[18−20] LANL2DZ pseudopotentials were used on platinum and phosphorus atoms, with LANL2DZ basis set for platinum and 3−21G* for all other atoms.[21,22] The model compound for **polymer 3** and the spacer **1-para** were optimized before the time-dependent density-functional theory (TDDFT) calculations. Only the relevant (stronger oscillator strength and wave function coefficients) molecular orbitals are shown. All computations were performed without symmetry constraints.

Results and Discussion

Synthesis and Characterization. Spacers **1-para** and **1-ortho** are prepared from the condensation of *para*- and *ortho*-ethynyl(trimethylsilane)aniline with duroquinone, respectively (Scheme 2).

Crystals suitable for X-ray crystallography were obtained by slow evaporation of a DMF solution at room temperature

(12) Connelly, N. G.; Geiger, W. E. *Chem. Rev.* **1996**, *96*, 877.
(13) (a) Flack, H. D.; Blanc, E.; Schwarzenbach, D. *J. Appl. Crystallogr.* **1992**, *25*, 455–459. (b) Gabe, E. J.; Le Page, Y.; Charland, J.-P.; Lee, F. L.; White, P. S. *J. Appl. Crystallogr.* **1989**, *22*, 384–387.
(14) Sheldrick, G. M. *SHELXS-97*, Release 97−2; University of Göttingen: Göttingen, Germany, 1997.

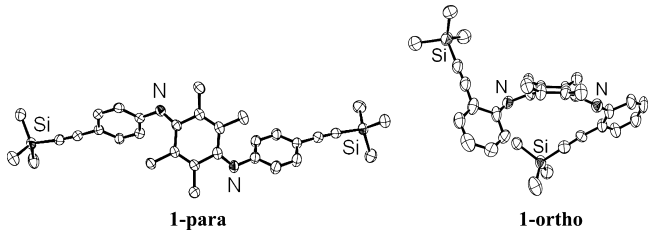

Figure 1. Oak Ridge Thermal Ellipsoid Plot (ORTEP) representation of spacers **1-para** and **1-ortho**. The ellipsoids are shown at 30% probability and the H-atoms are not shown for clarity.

Scheme 3. Synthesis of the Polymer **3** and the Model Compound **4**

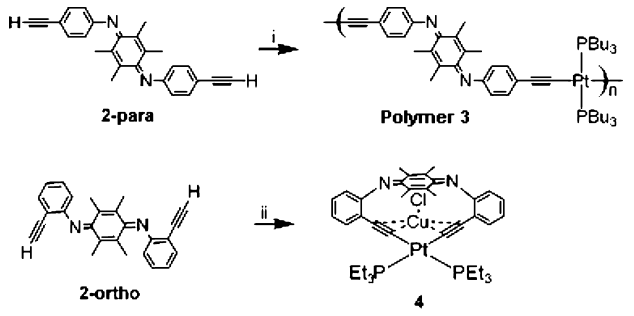

(Figure 1). The short C≡C (1.213(5) and 1.211(5) Å) and C=N distances (1.293(4) and 1.284(4) Å) witness the ethynyl and imine functions.

The chemical yields are 68 and 75% for **1-para** and **1-ortho**, respectively. The possible explanation for the lower isolated yields is the presence of incomplete reactions at the monosubstitution step where mono-one-monoimine species (**1′-ortho** and **1′-para**) were observed. These two intermediates were isolated and characterized by X-ray crystallography (see Supporting Information). **1-para** and **1-ortho** were desilylated using K_2CO_3 in methanol affording **2-para** and **2-ortho**, respectively.

Polymer **3** is prepared by a deshydrohalogenation reaction between **2-para** and *trans*-$PtCl_2(PBu_3)_2$ in diisopropylamine and CuI in a 83% yield (Scheme 3). The polymer exhibits a singlet at 6.9 ppm in the $^{31}P\{^1H\}$ NMR spectra flanked with satellites ($^1J_{Pt-P} = 2360$ Hz) in $CDCl_3$. These data compare favorably to that of *trans*-$Pt(PBu_3)_2(C{\equiv}CPh)_2$ ($\delta = 4.14$ ppm, $^1J_{Pt-P} = 2350$ Hz),[23] hence confirming the *trans*-geometry of the Pt-containing unit. Similarly, the 1:1 ratio of ligand versus Pt-containing starting materials is confirmed by ^1H NMR (using the integrated signals for aromatic protons vs Bu). An IR band observed at ~2100 cm^{-1} is also diagnostic for the coordination of C≡C onto Pt in the *trans*-[−C≡C−PtL_2−C≡C−]-containing polymers (L = PBu_3).[23] The different IR (2097 cm^{-1}) and Raman (2106 cm^{-1}) C≡C stretching frequencies (see Supporting Information) indicate the presence of a center of inversion about Pt, expected for the *trans*-geometry (D_{2h}).

Because the amorphous polymer **3** was not crystallizable, a model compound of very low molecular weight was prepared as a cyclic mononuclear complex. The mononuclear cyclic compound **4** was hence prepared in the same way as polymer **3** using the *cis*-$PtCl_2(PEt_3)_2$ complex instead of *trans*-$PtCl_2(PBu_3)_2$ (Scheme 3). The reason for this choice is that in our previous work it was shown that the *cis*- and the *trans*-$PtCl_2(PEt_3)_2$ complexes kept their geometry in the polymer.[4] We find that the *cis*-$PtCl_2(PBu_3)_2$ does not. In addition, the choice of butyl groups in polymer **3** instead of ethyl groups as in **4** was to improve the solubility of the polymer and consequently, the molecular weight. Suitable crystals for X-ray analysis were obtained for **4**. The presence of CuCl (Cu coming from CuI, and Cl coming from the starting Pt-material) inside the bite of the *cis*-$Pt(C{\equiv}C)_2$ structure was detected in this case, a situation that is commonly observed in the literature.[24] This result differs from a similar complex reported earlier by us where the quinone diimine fragment is substituted by 4 methoxy groups instead of methyl (where no CuCl is detected).[4] The elemental analysis is consistent with the presence of CuCl (Figure 2), as well as the DMF crystallization molecule. The absence of CuX in the previous structure may likely be due to the presence of methoxy groups (instead of methyl) inducing steric hindrance. Similarly, the presence and absence of Cu-containing fragment in compound **4** and polymer **3** (as noted from the chemical analyses), respectively, may be due to the favorable *cis*-chelating arrangement of the ethynyl donors in **4** which is not possible in the polymer.

The GPC analysis (see Supporting Information) for polymer **3** indicates that $M_n = 18500$ (corresponding to about 19 units), $M_w = 25000$ (PD = 1.37). The TGA trace (at a

(15) Sheldrick, G. M. *SHELXL-97*, Release 97−2; University of Göttingen: Göttingen, Germany, 1997.
(16) Flack, H. D. *Acta Crystallogr.* **1983**, *A39*, 876–881.
(17) Frisch, M. J.; Trucks, G. W.; Schlegel, H. B.; Scuseria, G. E.; Robb, M.; Cheeseman, J. R.; Montgomery, J. A.; Vreven, J. A.; Kudin, K. N.; Burant, J. C.; Millam, J. M.; Iyengar, S. S.; Tomasi, J.; Barone, V.; Mennucci, B.; Cossi, M.; Scalmani, G.; Rega, N.; Petersson, G. A.; Nakatsuji, H.; Hada, M.; Ehara, M.; Toyota, K. ; Fukuda, R.; Hasegawa, J.; Ishida, M.; Nakajima, T.; Honda, Y.; Kitao, O.; Nakai, H.; Klene, M.; Li, X.; Knox, J. E.; Hratchian, H. P.; Cross, J. B.; Adamo, C.; Jaramillo, J.; Gomperts, R.; Stratmann, R. E.; Yazyev, O.; Austin, A. J.; Cammi, R.; Pomelli, C.; Ochterski, J. W.; Ayala, P. Y.; Morokuma, K.; Voth, G. A.; Salvador, P.; Dannenberg, J. J.; Zakrzewski, V. G.; Dapprich, S.; Daniels, A. D.; Strain, M. C.; Farkas, O.; Malick, D. K.; Rabuck, A. D.; Raghavachari, K.; Foresman, J. B.; Ortiz, J. V.; Cui, Q. ; Baboul, A. G. ; Clifford, S. ; Cioslowski, J.; Stefanov, B. B.; Liu, G.; Liashenko, A.; Piskorz, P.; Komaromi, I.; Martin, R. L.; Fox, D. J.; Keith, T.; Al-Laham, M. A.; Peng, C. Y.; Nanayakkara, A.; Challacombe, M.; Gill, P. M. W.; Johnson, B.; Chen, W.; Wong, M. W.; Gonzalez, C.; Pople, G. A., *Gaussian 03*, Revision C.02; Gaussian,Inc.: Wallingford, CT, 2004.
(18) Becke, A. D. *J. Chem. Phys.* **1993**, *98*, 5648–5652.
(19) Lee, C.; Yang, W.; Parr, R. G. *Phys. Rev. B: Condens. Matter Mater. Phys.* **1988**, 785–789.
(20) Miehlich, B.; Savin, A.; Stoll, H.; Preuss, H. *Chem. Phys. Lett.* **1989**, *157*, 200–206.
(21) Dobbs, K. D.; Hehre, W. J. *J. Comput. Chem.* **1986**, *7*, 359–378.
(22) (a) Dobbs, K. D.; Hehre, W. J. *J. Comput. Chem.* **1987**, *8*, 861–879. (b) Dobbs, K. D.; Hehre, W. J. *J. Comput. Chem.* **1987**, *8*, 880–893.
(23) (a) Sonogashira, K.; Fujikura, Y.; Yatake, T.; Toyoshima, N.; Takahashi, S.; Hagihara, N. *J. Organomet. Chem.* **1978**, *145*, 101–108. (b) Long, N. J.; White, A. J. P.; Williams, D. J.; Younus, M. *J. Organomet. Chem.* **2002**, *649*, 94–99.
(24) (a) Adams, C. J.; Raithby, P. R. *J. Organomet. Chem.* **1999**, *578*, 178–185. (b) Lang, H.; del Villar, A.; Rheinwald, G. *J. Organomet. Chem.* **1999**, *587*, 284–289. (c) Wong, W.-Y.; Lu, G.-L.; Choi, K.-H. *J. Organomet. Chem.* **2002**, *659*, 107–116. (d) Ara, I.; Berenguer, J. R.; Eguizabal, E.; Fomies, J.; Gomez, J.; Lalinde, E. *J. Organomet. Chem.* **2003**, *670*, 221–234. (e) Ara, I.; Berenguer, J. R.; Eguizabal, E.; Fomies, J.; Gomez, J.; Lalinde, E.; Martin, A. *Eur. J. Inorg. Chem.* **2001**, 1631–1640. (f) Yamazaki, S.; Deeming, A. J. *J. Chem. Soc., Dalton Trans.* **1993**, 3051–3058. (g) Fomies, J.; Lalinde, E.; Martin, A.; Moreno, M. T. *J. Organomet. Chem.* **1995**, *490*, 179–188.

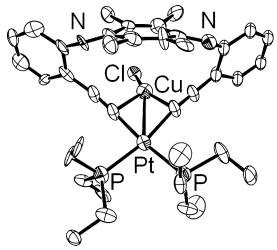

Figure 2. ORTEP representation of compound **4**. The ellipsoids are shown at 30% probability and the H-atoms and DMF solvent molecule are not shown for clarity. Selected distances: Pt−Cu, 2.955(4); Cu−Cl, 2.234(6); Cu−C, 2.037(19), 2.192(17); C≡C, 2.064 (16), 1.94(2); Pt−P, 2.311(5), 2.297(6) Å.

heating rate of 3 °C min^{-1} under Ar) exhibits a first weight loss temperature of about 35% decomposition at temperatures exceeding 280 °C. This decomposition could be assigned to the loss of various number of alkyl chains on the phosphine ligands from the Pt polyine chain.[2a] The DSC trace for polymer **3** exhibits a weak T_g (glass transition) at 87.0 °C.

Electrochemical Results. In a pure DMF/$[NBu_4][PF_6]$ electrolyte, **1-para** shows only a chemically irreversible reduction at $E_{pc} = -1.05$ V versus SCE to which an anodic wave is coupled at $E_{pa} = -0.51$ V. Upon addition of trifluoroacetic acid (TFA), reduction of **1-para** appears at a much more positive potential, consistent with the behavior expected for the reduction of diphenyl-1,4-benzoquinonediimine complexes under acidic conditions.[5a] The CV response of this system is shown in Figure 3 (top). The dashed line in this figure shows that a small prewave present at approximately 0.40 V produced an anodic product wave at 1.0 V on the reverse sweep. However, the main cathodic and coupled anodic waves for **1-para** under these conditions (see solid line in Figure 3, top) occurred at about 0 and 0.86 V, respectively. Owing to the broadness of the cathodic wave and its position near the rising portion of the TFA reduction, its potential was better determined by DPV, with which a value of 0.14 V was obtained. Although **1-para** exhibits a diffusion-controlled reduction in this medium, its cathodic electrochemistry appears to be more complex than that of previously reported systems lacking the *p*-alkynyl substituent.[5a]

The cathodic behavior of the polymer **3** was more straightforward. Whereas it was electrochemically silent between 1.2 and −1.8 V in pure DMF/$[NBu_4][PF_6]$, a single chemically reversible reduction was seen for **3** after addition of TFA, with $E_{pc} = 0.44$ V and $E_{pa} = 0.54$ V at a CV scan rate of 0.2 V s^{-1} (Figure 3, middle). The broadening of the CV response in the more negative potential region arises from small cathodic features that are not likely to be important to the basic voltammetric behavior of **3**. DPV scans improved visualization of the primary cathodic wave (Figure 3, bottom) and showed the minor secondary waves to be only about 10−15% of the current seen for the main peak. According to the DPV result, the $E_{1/2}$ of **3** in this medium is 0.47 V versus SCE. More importantly, the narrowness of the DPV wave showed that it arose from a reversible *two-electron* process.

The theoretical widths at half-height for Nernstian processes are approximately 90 mV for a one-electron process

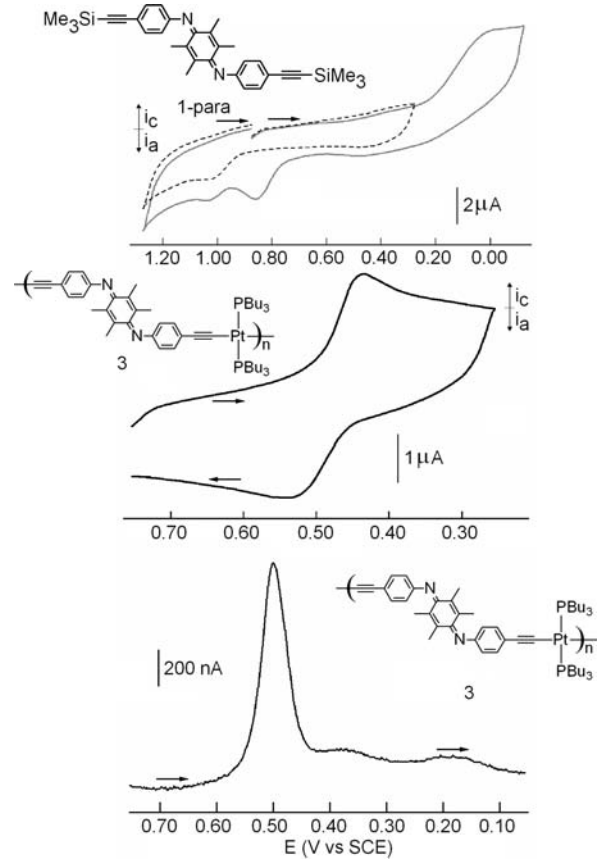

Figure 3. (Top) Cyclic voltammogram of 1 mM **1-para** in DMF/0.1 M $[NBu_4][PF_6]$ containing 2.7 M trifluoracetic acid, 2 mm Pt electrode, scan rate 0.2 V s^{-1}. Dashed and solid lines show scans to different switching potentials, and both scans were initiated at 0.9 V. (Middle) Cyclic voltammogram of 1.1 mM **3** in DMF/0.1 M $[NBu_4][PF_6]$ containing 2.7 M trifluoracetic acid, 2 mm Pt electrode, scan rate 0.2 V s^{-1}. (Bottom) Differential pulse voltammogram of 1.1 mM **3** in DMF/0.1 M $[NBu_4][PF_6]$ containing 2.7 M trifluoracetic acid, 2 mm Pt electrode, scan rate 0.05 V s^{-1}, pulse height 25 mV.

and 45 mV for a two-electron process.[25] The value of 55 mV observed for **3** clearly establishes that its cathodic wave arises from a two-electron process. Given the acidic conditions and the well-established behavior of diphenyldiimine analogues, the reversible reaction almost certainly also involves gain and loss of protons. Keeping in mind that **3** is a polymer with approximately 19 units, the stoichiometry of the redox process may be written as involving the repeating units **3′**, each of which undergoes the two-electron process of eq 1:

$$\mathbf{3'} + 2e^- + 2H^+ \rightleftharpoons \mathbf{3'}H_2 \qquad E_{1/2} = 0.47 \text{ V vs SCE} \quad (1)$$

Less certain is the question of whether or not there is electronic communication between the repeating units. The present data are consistent with either of two extremes. Certainly, the fact that the fundamental redox behavior of **3** (a reversible two-electron process in acidic media) is similar to that of PANI polymers[26] supports the idea that the Pt-based polymer **3** may also be conducting. Similar voltam-

(25) Bard, A. J.; Faulkner, L. R. *Electrochemical Methods*, 2nd ed.; John Wiley & Sons: New York, 2001; p 293.
(26) Ping, Z.; Nauer, G. E.; Neugebauer, H.; Theiner, J.; Nechel, A. *J. Chem. Soc., Faraday Trans.* **1997**, *93*, 121–129.

metry would be observed, however, if the two-electron process is essentially localized on each diphenyldiimine linkage. The case of mutually isolated redox sites has been treated in detail for vinyl ferrocene polymers.[27]

In any case, the $E_{1/2}$ of the second reduction (presumably $\mathbf{3'}H + e^- \rightleftharpoons \mathbf{3'}H_2$) must be *more positive* than that of the first reduction ($\mathbf{3'} + e^- \rightleftharpoons \mathbf{3'}H$) to result in the observed DPV peak width. On the basis of the results of simulation results of Richardson and Taube,[28] the "potential inversion"[29] of the second reduction must be at least 50 mV.

To verify that the observed electrochemical process was not due to protonation of the ethynyl group, the model compound **5**, *trans*-$Pt(PBu_3)_2(C{\equiv}CPh)_2$, was investigated as well. The electrochemical properties of this compound are known but not in the presence of acid.[30,31] In the absence of acid, this compound exhibits an irreversible oxidation peak at ~1.2 V versus Ag/AgCl, and a transfer of 1.43 ± 0.21 electron in a benzene/acetonitrile mixture containing **5** was observed.[31] In this work we obtained the same results (see Supporting Information). In the presence of 2 M TFA, no change in the CV was observed, indicating that the electrochemical process observed for polymer **3** is due to the presence of the diimine function.

Compound **4** exhibits ill-defined traces (see Supporting Information) suggesting that irreversible processes are taking place. It is suspected that an intramolecular transformation occurs.[32] No further investigation was undertaken on this compound.

Absorbance and Luminescence Spectra. The absorption spectra for **1-para** and **2-para** are characterized by a broad low-energy band located between 400 and 600 nm with maxima at 446 ($\varepsilon = 5690$) and 440 nm ($\varepsilon = 7100$ dm^3 mol^{-1} cm^{-1}), respectively (Figure 4). Their assignments are made on the basis of density-functional theory (DFT) and TDDFT calculations.

As no X-ray structure of polymer **3** is available, a calibration of the methodology is necessary. So, a comparison of the optimized geometry data of **1-para** with the X-ray structure is performed (Figure 5). The difference between the X-ray results and the computed data of the symmetric optimized geometry ranges from 0.00 to about 0.02 Å. Such comparison is reasonable. Two exceptions are observed. First, the calculated Si−C bond distance is longer than the experimental data (by about 0.043 Å). This difference bears no consequence since the atomic contribution of the Si atoms to the frontier molecular orbitals (MOs) is practically nil

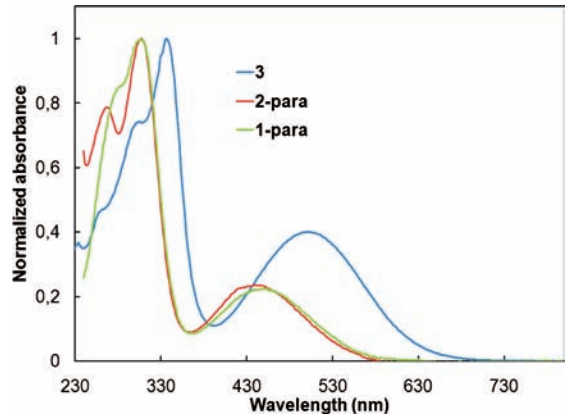

Figure 4. Normalized absorption spectra of **1-para** ($\lambda_{max} = 446$ nm, $\varepsilon = 5690$), **2-para** ($\lambda_{max} = 440$ nm, $\varepsilon = 7100$) and **polymer 3** ($\lambda_{max} = 502$ nm, $\varepsilon = 23400$) in 2-MeTHF.

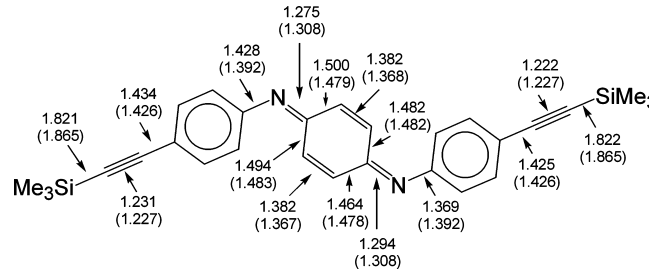

Figure 5. Comparison of selected bond distances for **1-para** between the X-ray (numbers not in parentheses) and the optimized geometry data (numbers in parentheses).

(Figure 6). Second, the X-ray C=N and C−N bond lengths on one side of the molecule exhibit larger discrepancies (i.e., 0.033 and 0.036 Å, respectively). The large X-ray C−N=C−C dihedral angle of 61.9° in comparison with 12.9° for the other side explains this difference. The latter angle compares more favorably with the computed angles for the "gas phase" optimized geometry (18.0 and 17.5°). The crystal packing plays a role for this dihedral angle, hence stressing the importance of comparing both the X-ray and optimized geometry data.

Figure 6 exhibits the computed frontier MOs for **1-para** using the X-ray and optimized geometry data. The highest occupied molecular orbital (HOMO), HOMO-1, and lowest unoccupied molecular orbital (LUMO) are placed at −0.210, −0.199, and −0.088 au, respectively (calculated from X-ray data). The LUMO is mainly composed of atomic contributions arising from the π-system of the quinone diimine (with some minor contributions of the $C{\equiv}CC_6H_4$ units), suggesting conjugation. The HOMO is also composed of a π-system located on the $C{\equiv}CC_6H_4$ ends of the spacer but mostly localized on the end exhibiting the smallest C−N=C−C dihedral angle. Moreover, this MO exhibits some contributions of the π-system of the central quinone diimine residue, also suggesting conjugation. Similarly, the HOMO-1 is composed of the π-system, but the largest electronic density is found on the other end of the molecule (i.e., largest dihedral angle). The calculated HOMO, HOMO-1, and LUMO of the optimized geometry of **1-para** are placed at −0.210, −0.196, and −0.104 au, respectively. The computed MOs exhibit the same characteristics as that described for

(27) Flanagan, J. B.; Margel, S.; Bard, A. J.; Anson, F. C. *J. Am. Chem. Soc.* **1978**, *100*, 4248.
(28) Richardson, D. E.; Taube, H. *Inorg. Chem.* **1981**, *20*, 1278.
(29) Evans, D. H.; Lehmann, M. W. *Acta Chem. Scand.* **1999**, *53*, 765.
(30) Kershman, J. R.; Paris, K. E.; Stamey, J. A.; Pyati, R. *J. Electroanal. Chem.* **2006**, *597*, 87–94.
(31) Kondrachova, L.; Paris, K. E.; Sanchez, P. C.; Vega, A. M.; Pyati, R.; Rithner, C. D. *J. Electroanal. Chem.* **2005**, *756*, 287–294.
(32) During the course of this study, a minor but very interesting tricyclized new compound was isolated as crystals in the synthesis of **4** (see ORTEP in the Supporting Iinformation). It is issued from an intramolecular addition of the ethynyl fragment onto the electron-rich olefin of the diimine cycle (Figure 2). It is believed that this compound is prone to intramolecular reactivity upon electrochemical processes due to the proximity of the olefins and ethynyl groups.

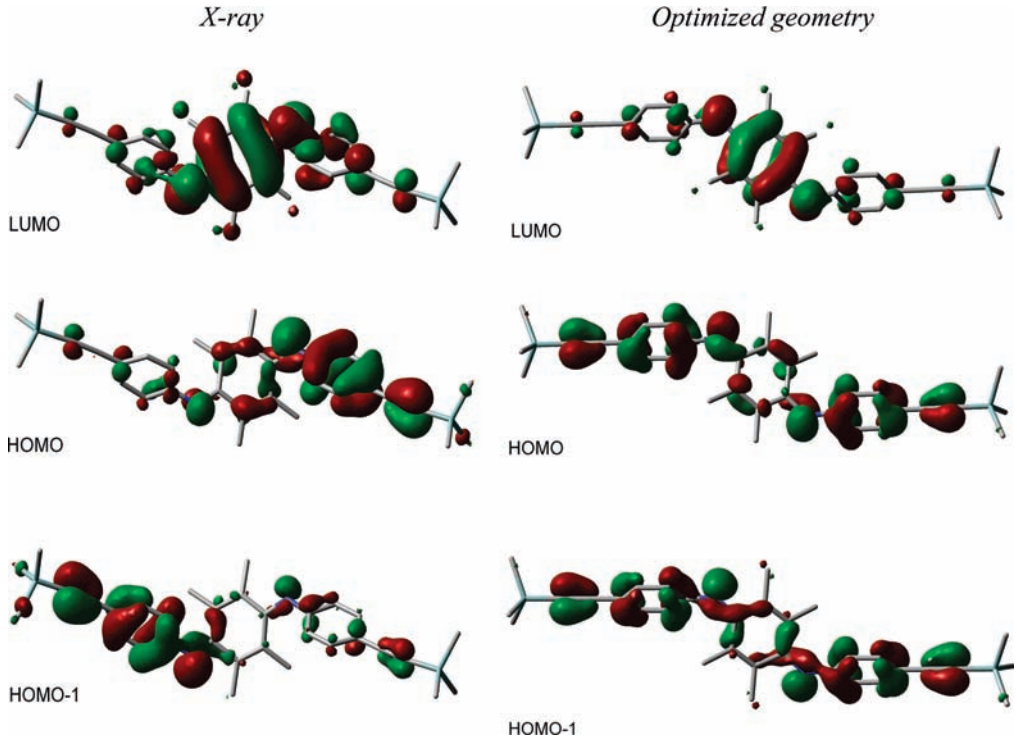

Figure 6. Frontier MOs for **1-para** computed using X-ray and optimized geometry data.

Table 2. Computed Spectral Parameters for the Two First Singlet-Singlet Transitions for **1-para** Using the X-ray and Optimized Geometry Data

	X-ray structure	optimized geometry
1st transition energy (eV)	2.47	2.03
position of the 0−0 peak (nm)	501	610
oscillator strength	0.49	0.60
assignment	HOMO−LUMO (CT)	HOMO−LUMO (CT)
2nd transition energy (eV)	2.61	2.12
position of the 0−0 peak	476	584
oscillator strength	0.021	0.012
assignment	HOMO-1−LUMO (CT)	HOMO-1−LUMO (CT)

the X-ray-based generated MOs, except that the atomic contributions are evenly distributed over both sides of the molecule owing to the C_2-symmetry of this "gas phase" geometry. All in all, the HOMO/LUMO and HOMO-1/LUMO transitions are predicted to be charge transfers (CT) from the π-systems of the C≡CC_6H_4 residues to the central quinone diimine π^* MO.

In our previous work, it was demonstrated that the position of the CT absorptions is directly a function of the C−N=C−C dihedral angle, where the CT transition red-shifts with the decrease in angle.[4] TDDFT was employed to localize the CT bands using both the X-ray and optimized geometry data for **1-para** (Table 2). The two computed lowest singlet−singlet 0−0 absorptions using the X-ray data are found at 501 and 476 nm resulting from the HOMO → LUMO and HOMO-1 → LUMO transitions with calculated oscillator strengths of 0.49 and 0.021, respectively. Similarly, the computed analogue transitions, using the optimized geometry data, are placed at 610 and 584 nm, with oscillator strengths of 0.60 and 0.012, respectively. Experimentally, the lowest energy band is located at 446 nm exhibiting a long tail spreading

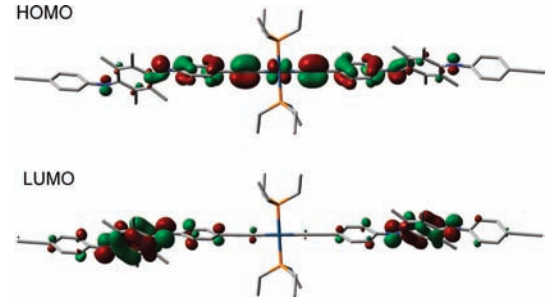

Figure 7. HOMO and LUMO representation for the model compound *trans*-(2-**para**)-Pt(PEt_3)$_2$-(**2-para**). Selected average distances: Pt−C, 2.018; Pt−P, 2.361; C≡C, 1.229; C=N, 1.300; C=C, 1.359; C−Cquinone, 1.481. The C−N=C−C dihedral angles are 18.93, 18.75, 16.08, 15.51°.

down to ∼580 nm. The comparison between the experimental and optimized geometry data is reasonable since the exact dihedral angle for the spacer in solution is unknown. As the absorption spectra of **1-para** and **2-para** are very similar, no computation was performed in this case.

The absorption spectrum of polymer **3** (Figure 4) is characterized by a broad low-energy absorption (at 502 nm; $\varepsilon = 24300$ dm^3 mol^{-1} cm^{-1}). The red shift of the low energy band is indicative of conjugation across the chain (∼19 units long). This observation is also corroborated by the conjugation deduced from the DFT calculations below. Interestingly, the absorptivity drastically increased. To propose an assignment and to corroborate the conjugation across the polymer chain, DFT and TDDFT computations were also performed on a model compound *trans*-(2-**para**)-Pt(PEt_3)$_2$-(**2-para**). Figure 7 exhibits the HOMO and LUMO for this model compound for an optimized geometry. The HOMO exhibits an atomic contribution mainly localized in the Pt(C≡CC_6H_4)$_2$ fragment and some minor atomic components placed on the quinone diimine residue, again consistent with conjugation,

which in turn, is also consistent with the computed C−N=C−C dihedral angles in this model which range from 15.5 to 19.0°, similar to the spacer **1-para** above. The ends of the chain ($HC{\equiv}CC_6H_4$) exhibit no contribution at all. The LUMO exhibits a large atomic contribution at the benzoquinone diimine center and very minor components from the $Pt(C{\equiv}CC_6H_4)_2$ units are observed. These computations support the CT assignment.

The TDDFT calculations predict a CT transition energy of 1.92 eV corresponding to a position of the 0−0 peak at 647 nm. The measured absorption band exhibits a maximum at 502 nm and a long tail spreading down to 680 nm (Figure 4). In our previous work on the tetramethoxy analogue (see data in Supporting Information of reference 4), when the solvent (THF) was included in the TDDFT computations, a red shift of 20 nm (i.e., 280 cm^{-1}) from 597 nm (16750 cm^{-1}; gas phase) to 607 nm (16470 cm^{-1}; with THF) of the 0−0 peak was computed. If we transposed this corresponding 20 nm shift (i.e., 280 cm^{-1}) to the gas phase 647 nm (15460 cm^{-1}) calculated value, an estimated value of 659 nm (i.e., 15180 cm^{-1}) is anticipated. Such value (659 nm) is within the tail of the absorption band (Figure 4). Again, this comparison is reasonable. The computed oscillator strength is 1.37 (larger than that computed for **1-para** above), which is consistent with the increase in the observed absorbtivity. The calculated red shift of the CT band going from **1-para** to this model compound is again consistent with extended conjugation. Moreover, the 502 nm experimental value for the CT band of polymer **3** is blue-shifted in comparison with that for the tetramethoxy analogue (535 nm; see Table 3 of reference 4). This shift is also consistent with the CT assignment as the methyl group is a better σ-donor by induction.

Polymer **3** is also found to be non-luminescent in solution and in the solid state at 298 and 77 K, meaning that the CT state is deactivated efficiently to ground-state via nonradiative pathways. On the other hand, spacer **2-para** in solution at 77 K exhibits higher energy fluorescence and phosphorescence (spectra and photophysical data are placed in the Supporting Information) arising from the $-C_6H_4-C{\equiv}CH$ residues. These emission bands were also observed for the analogue spacers bearing the methoxy groups and are explained by a weak electronic communication between the $-C_6H_4-C{\equiv}CH$ residues with the quinone diimine fragment in the excited state. No complete analysis was performed in this work since this is not the purpose of this work and since it is fully explained elsewhere.[4]

Conclusion

This tetramethylbenzoquinone diimine-containing conjugated organometallic polymer was prepared and characterized along with a cyclic compound **4**. It does not bear methoxy groups on the quinone diimine as previously reported, decreasing hence the number of trapping sites for H^+ ions, and does not decompose when the acid concentration increase up to 2 M. Indeed, the cyclic voltammogram of polymer **3** was investigated in the presence and absence of H^+ ions. In the presence of H^+, a chemically reversible but electrochemically irreversible redox process appears and is clearly associated to the quinone diimine/diamine couple analogous to conducting PANI.[26] The deep coloration of the new and non-luminescent polymer is due to a low energy CT absorption; a CT process of the type $Pt(PBu_3)_2(C{\equiv}CC_6H_4)_2 \rightarrow$ quinone diimine. This CT band is located in the red region of the visible spectra (spreading from 400 to 650 nm in polymer 3), which gives the polymer the possibility to act as a good antenna for solar light collection for applications in solar energy conversion. On the basis of these optical and electrochemical findings, polymer **3** may be a potential candidate for the design of novel conducting polymers resembling that of an organometallic version PANI and photovoltaic cells.

Acknowledgment. This work was supported by the Natural Science and Engineering Research Council of Canada (NSERC). The authors thank Dr. Normand Pothier, Dr. Jérôme Babin, Dr. Smail Dahmane, Dr. Regina Zamojska, and Anne Brisach-Wittmeyer for the measurements of the RAMAN spectra, of the GPC traces, the DSC and ATG traces, and the preliminary electrochemical cyclic voltammograms, respectively.

Supporting Information Available: RAMAN and IR spectra in the region of the C≡C stretching frequencies for polymer **3**, GPC trace of polymer **3**, ATG trace of polymer **3**, ORTEP representation for **1′-para** and **1′-ortho**, emission, excitation and absorption spectra of **2-para** in 2-MeTHF at 77 K, photophysical data of compound **2-para** at 77 K, oxidation and reduction of Pt compound **4**, and one minor product isolated during the synthesis of **4**. This material is available free of charge via the Internet at http://pubs.acs.org.

IC800857V